

Brain-aligning of semantic vectors improves neural decoding of visual stimuli

Shirin Vafaei¹, Ryohei Fukuma^{1,2}, *Takufumi Yanagisawa^{1,2,3}, Huixiang Yang², Satoru Oshino^{1,3}, Naoki Tani^{1,3}, Hui Ming Khoo^{1,3}, Hidenori Sugano⁴, Yasushi Iimura⁴, Hiroharu Suzuki⁴, Madoka Nakajima⁴, Kentaro Tamura^{5,6}, Haruhiko Kishima¹

¹Department of Neurosurgery, Graduate School of Medicine, Osaka University, Suita, Japan

²Institute for Advanced Co-Creation Studies, Osaka University, Suita, Japan

³Osaka University Hospital Epilepsy Center, Suita, Japan

⁴Department of Neurosurgery, Juntendo University, Tokyo, Japan

⁵Department of Neurosurgery, Nara Medical University, Kashihara, Japan

⁶Department of Neurosurgery, National Hospital Organization, Nara Medical Center, Nara, Japan

***Corresponding author**

Takufumi Yanagisawa

Address: 2-2 Yamadaoka, Suita, Osaka 565-0871, Japan

Tel.: +81-6-6879-3652

Fax: +81-6-6879-3659

E-mail: tyanagisawa@nsurg.med.osaka-u.ac.jp

Abstract

The development of algorithms to accurately decode of neural information is a long-standing effort in the field of neuroscience. Brain decoding is typically employed by training machine learning models to map neural data onto a preestablished vector representation of stimulus features. These vectors are usually derived from image- and/or text-based feature spaces.

Nonetheless, the intrinsic characteristics of these vectors might be fundamentally different than those encoded by the brain, limiting the ability of algorithms to accurately learn this mapping. To address this issue, here, we propose a representation learning framework, called brain-aligning of semantic vectors, that fine-tunes pretrained feature vectors to better align with the structure of neural representations of visual stimuli in the human brain. We trained this model with functional magnetic resonance imaging (fMRI) data representing 150 visual stimulus categories; then, we performed zero-shot brain decoding on 1) fMRI, 2) magnetoencephalography (MEG), and 3) electrocorticography (ECoG) data reflecting neural representations of visual stimuli. By using fMRI-based brain-aligned vectors, the zero-shot decoding accuracy all three neuroimaging datasets increased. This finding underscores the potential of leveraging a richer array of brain-derived features to increase the performance of brain decoding algorithms.

Introduction

The development of brain decoding algorithms is essential for advancing brain-machine interfaces (BMIs)¹⁻⁴ that enable precise communication and motor control for individuals with speech or motor impairments. Simultaneously, these algorithms offer a unique opportunity to delve into the intricacies and fundamental mechanisms underlying information processing in the human brain⁵⁻¹⁰. Furthermore, precise decoding can improve the effectiveness of neurofeedback systems by enabling the precise decoding of cognitive patterns and delivering real-time neurofeedback, thereby assisting patients in the refinement of their cognitive and emotional faculties¹¹⁻¹⁴.

Previous studies have shown that neural activity patterns can be decoded to reveal *information* about perceived or imagined visual stimuli (i.e., images). This *information* can take the form of semantic attributes^{10,15-18}, category-level classes^{5,7,15,19,20} or even reconstructed visual representations of the images²¹⁻²⁴. Decoding typically involves representing a specified attribute as a pretrained feature vector, often derived from object recognition neural networks^{15,25}, multimodal models^{26,27} or word co-occurrence statistics^{12,28-30}. Afterward, machine learning models are trained to map neural activity patterns onto these feature vectors.

While pretrained feature vectors have enabled brain decoding with above-chance accuracy, current models are still limited in accurately learning this mapping, particularly in zero-shot decoding scenarios, where decoders must generalize the learned information to novel semantic categories not encountered during training³¹. Given the impracticality of training decoders to understand all possible semantic categories, there is a pressing need for more robust and flexible decoding models.

In this study, we hypothesized that if the vectors used to represent stimuli are more aligned with how visual stimuli are encoded in the human brain, decoders can better learn the mapping of neural activity to feature vectors and even generalize this mapping to novel semantic categories using learned information encapsulated within the more brain-aligned vectors.

This idea was inspired by recent findings that use of brain-like or brain-integrated features can improve object recognition³², few-shot learning and anomaly detection tasks³³ and that consistent and high-performing latent spaces can be obtained by jointly learning from both behavioral and neural data³⁴. However, it has remained unclear whether semantic spaces with representations that are more aligned with neural encoding patterns can lead to more accurate zero-shot brain decoding.

To create a brain-aligned semantic vector representation of stimuli, we propose a framework called "brain-aligning of semantic vectors," which automatically reconstructs pretrained feature vectors while ensuring the second-order statistical features of its latent space are as similar as possible to those of brain activity patterns. The vectors extracted from the latent space of the autoencoder after training are called *brain-aligned semantic vectors*. We investigated whether utilizing these brain-aligned semantic vectors could improve zero-shot decoding¹⁵ and identification^{15,35} accuracy for 1) brain activity measured by the same neuroimaging technique used to fine-tune the pretrained feature spaces and 2) brain activity measured by a different neuroimaging technique than that used for fine-tuning.

Practically, we trained the brain-aligning framework by leveraging the brain activity patterns measured by fMRI and then tested the performance of the zero-shot decoding and identification of resulting brain-aligned vectors on the brain activity data measured by fMRI, MEG and ECoG. This cross-modality approach is critical because fMRI, MEG and ECoG

measure distinct aspects of brain activity: fMRI captures hemodynamic changes (BOLD signals)³⁶, ECoG records electrical activity³⁷, and MEG detects magnetic fields³⁸. Successful generalization across modalities would suggest that our vectors represent fundamental aspects of neural coding that are independent of specific measurement techniques.

Results

Brain-aligning of semantic vectors

We developed a multimodal learning autoencoder framework that takes a pretrained feature space and brain activity patterns corresponding to the visual stimuli dataset and aligns the feature space with the structure of visual representations in the human brain. For the selection of pretrained feature spaces, we leveraged two different feature spaces. The first is an image-based feature space including features from the image encoder model of CLIP²⁷, and the second is a text-based feature space including features from the *global vectors for word representation* (GloVe) model³⁰. The fMRI dataset used here to fine-tune the pretrained feature vectors was the generic object decoding (GOD) dataset¹⁵; this dataset contains fMRI recordings from 5 subjects viewing 1200 images of 200 distinct object categories selected from ImageNet³⁹. The GOD dataset has been specifically designed to prevent any overlap between the categories used for training and those used for testing, facilitating assessment of the zero-shot prediction capabilities of decoding models. Importantly, use of this dataset ensures that these models are evaluated on the basis of their ability to generalize to entirely new categories without prior exposure.

First, we extracted the original semantic vectors for each category in the GOD dataset (see methods) and represented each category by its corresponding pretrained feature vector. To

obtain the “brain-aligned semantic space”, we trained the autoencoder with a two-term objective function. The first term is a simple mean squared error (MSE) loss between true and predicted pretrained feature vectors (with the goal of reconstructing them). The second term is the MSE loss between the representational similarity matrix (RSM)³⁴ of the fMRI signals and the autoencoder’s latent space in each batch. Mathematically:

$$loss = \frac{1}{m} \sum_{i=1}^m \left[(\alpha) (y - y')^2 + (1 - \alpha)(RSM_l - RSM_b)^2 \right] \quad (1)$$

where y is the original semantic vector, y' is the reconstructed semantic vector, RSM_l is the RSM of the autoencoder’s hidden layer, RSM_b is the RSM of the corresponding brain activity patterns, and m is the number of samples in each batch. Finally, α is the hyperparameter that determines the extent of brain-aligning.

Given our aim to decode visual object categories, we used the fMRI data from the lateral occipital complex (LOC) to fine-tune pretrained feature vectors. The LOC is a region of the occipital lobe that is primarily responsible for visual processing of objects and shapes⁴⁰. Concurrently, to choose the appropriate pretrained feature vectors, we extracted the category-specific pretrained feature vectors of each category in the training data of the GOD dataset.

For each participant represented in the GOD dataset, pretrained feature vector and α , we trained a different autoencoder. When training the autoencoder for a particular participant (i.e., subject A) in the GOD dataset, we used the averaged RSM of fMRI brain signals of all other participants in the GOD dataset. We later used these brain-aligned vectors for decoding the fMRI brain signals of subject A to avoid information leakage. We trained autoencoders on a wide range of values of α ($\alpha = 0.0001, 0.001, 0.01, 0.1, 1$). We specifically included 1 as one of the values

to determine how excluding the brain-aligning part from this framework would affect the downstream analyses. Figure 1 shows an overview of the proposed workflow.

fMRI brain decoding and identification of visual stimuli

We performed brain decoding and identification for each feature space type and participant separately. Decoding was conducted by training linear regression models to map brain activity patterns to their corresponding feature vectors. For all samples and each unit in the semantic vectors, a separate set of linear regression models was trained. To evaluate decoding accuracy comprehensively, we employed both samplewise and dimensionwise correlation metrics.

Samplewise correlation, which was calculated as the average Pearson correlation between true and predicted vectors across all samples and subjects, is a global measure of the model's ability to reconstruct entire brain activity patterns^{6,7,41,42}. In contrast, dimensionwise correlation, which was calculated as the average Pearson correlation across feature units, assesses the model's capacity to capture fine-grained representational details at the level of individual semantic features^{15,17,43,44}. This metric is essential for understanding how well the model decodes specific semantic or conceptual features embedded within the neural representations.

Furthermore, we evaluated the models' identification accuracies to assess their ability to correctly classify stimuli on the basis of the predicted feature vectors. This evaluation is critical for determining the practical utility of decoding models used in real-world applications, such as brain-machine interfaces or neurofeedback systems^{6,35}. For this purpose, we computed the Pearson correlation coefficient between the predicted semantic vector and all other candidate vectors. The accuracy is defined as the percentage of candidate categories whose correlation with

the predicted vector is lower than the correlation between the actual true and predicted vectors. The final identification accuracy is determined by averaging the identification accuracies across all categories and subjects in the test dataset. Figure 2 shows an overview of decoding and identification algorithms.

We then evaluated the performance of our decoding and identification methods relative to chance. Specifically, we compared the decoding and identification results obtained from the original data with those obtained from shuffled data. For samplewise and dimensionwise decoding, shuffled accuracy was determined by correlating the predicted feature vectors with the randomly shuffled true feature vectors. For identification, the shuffled accuracy was obtained by correlating the predicted vectors with both the shuffled true vector and all other candidate vectors. The shuffled identification accuracy was then defined as the percentage of candidate categories whose correlation with the predicted vector was lower than the correlation between the shuffled true and predicted vectors.

Figure 3 presents the fMRI decoding and identification results for both perceived and imagined stimuli, using either CLIP-based or GloVe-based feature vectors. For all analyses (samplewise decoding, dimensionwise decoding and identification), the real accuracy was significantly greater than the corresponding shuffled accuracy (one-sided t -test after Fisher's z -transform, $P < 0.05$; see Supplementary Tables 1-48 for exact values).

Furthermore, we observed that decoding accuracy depends on the degree of brain-aligning. The samplewise decoding accuracies for different values of α were significantly different for both the perceived image data (CLIP-based feature vectors, $F_{(5, 24)} = 79.900$, $P < 0.001$; GLoVe-based feature vectors, $F_{(5, 24)} = 321.611$, $P < 0.001$; one-way ANOVA, Bonferroni corrected significance level = $0.05/12$; Fig. 3a) and the imagined image data (CLIP-based feature

vectors, $F_{(5, 24)} = 54.716, P < 0.001$; GLoVe-based feature vectors, $F_{(5, 24)} = 93.186, P < 0.001$; one-way ANOVA, Bonferroni corrected significance level = 0.05/12; Fig. 3b).

Notably, within the CLIP-based vectors, the decoding accuracies corresponding to the brain-aligned vectors initially decreased with as α values decreased from 1 (Perception, $P < 0.01$, Tukey's HSD post hoc test, comparison between brain-aligned vectors with $\alpha = 10^{-1}$ and original feature vectors; imagined, $P < 0.05$, Tukey's HSD post hoc test, comparison between brain-aligned vectors with $\alpha = 1$ and original feature vectors and between $\alpha = 10^{-1}$ and original feature vectors; Fig. 3a and b). However, these accuracies gradually increased as α further decreased; particularly, brain-aligned vectors containing the most brain-related information ($\alpha = 10^{-3}$ and $\alpha = 10^{-4}$) yielded the highest decoding accuracies, significantly exceeding those of the original pretrained feature vectors and brain-aligned vectors with $\alpha = 1$ ($P < 0.01$, Tukey's HSD post hoc test; Fig. 3a and b). Within the GLoVe-based feature vectors, the decoding accuracies tended to increase as α decreased, achieving a significant improvement over the decoding accuracy of the original feature vectors (perceived images, $P < 0.01$, Tukey's HSD post hoc test; imagined images, $P < 0.01$, Tukey's HSD post hoc test; Fig. 3a and b). Additionally, decoding accuracies corresponding to the two top smallest values of alpha ($\alpha = 10^{-3}$ and $\alpha = 10^{-4}$) significantly increased compared with those of the brain-aligned vectors with $\alpha = 1$ (perceived images, $P < 0.01$, Tukey's HSD post hoc test; imagined images, $P < 0.01$, Tukey's HSD post hoc test; Fig. 3a and b).

Similarly, for the dimensionwise analysis of the perceived image data, the decoding accuracy of the brain-aligned vectors significantly differed with α (CLIP-based feature vectors, $F_{(5, 24)} = 9.620, P < 0.001$; GLoVe-based feature vectors, $F_{(5, 24)} = 5.050, P = 0.0027$; one-way ANOVA, Bonferroni corrected significance level = 0.05/12; Fig. 3c). Particularly, for the CLIP-

based results, the decoding accuracies tended to increase as α decreased, achieving a significant improvement over the decoding accuracy of the original feature vectors ($P < 0.05$, Tukey's HSD post hoc test; Fig. 3c). Concurrently, for the GLoVe-based feature vectors, the decoding accuracies of the two most brain-aligned vectors representing the most brain-related information ($\alpha = 10^{-3}$ and $\alpha = 10^{-4}$) significantly increased compared with the decoding accuracy of the original feature vectors ($P < 0.05$, Tukey's HSD post hoc test; Fig. 3c). However, the dimensionwise decoding accuracy of the imagined images did not significantly differ with α (CLIP-based feature vectors, $F_{(5, 24)} = 0.709$, $P = 0.6224$; GLoVe-based feature vectors, $F_{(5, 24)} = 0.760$, $P = 0.5875$; one-way ANOVA, Bonferroni corrected significance level = $0.05/12$; Fig. 3d).

Additionally, we observed that for both CLIP-based and GLoVe-based feature vectors, the identification accuracies across different groups of original and brain-aligned vectors did not show significant differences for different values of α (perceived images, CLIP-based feature vectors, $F_{(5, 24)} = 2.542$, $P = 0.0555$; perceived image data, GLoVe-based feature vectors, $F_{(5, 24)} = 0.8$, $P = 0.5606$; imagined images, CLIP-based feature vectors, $F_{(5, 24)} = 2.219$, $P = 0.0855$; imagined images, GLoVe-based feature vectors, $F_{(5, 24)} = 0.273$, $P = 0.9235$; one-way ANOVA, Bonferroni corrected significance level = $0.05/12$; Fig. 3e and f; see Supplementary Fig. 1 and Supplementary Tables 49-60 for exact values).

Moreover, we investigated whether brain-aligning could enhance the category discriminability of each feature unit, which we defined as the ratio of intercategory to intracategory variation in feature values (F statistic)¹⁵. Since the GloVe labels for all images within a category are identical, we only calculated category discriminability for the CLIP-based feature vectors. We computed the category discriminability of each feature unit across 19,933

ImageNet categories, with 8 images per category. The distribution of F values for the CLIP-based feature vectors revealed that the F values for the brain-aligned vectors significantly increased compared with the F values of the original feature vectors ($p < 0.001$; two-sided Wilcoxon rank-sum test), and the F values corresponding to the brain-aligned vectors with an α of 10^{-2} significantly increased compared with the F values of the feature vectors with $\alpha = 1$ ($p < 0.001$; Fig. 3g).

Generalization of decoding performance on other modalities: MEG and ECoG datasets

To assess the generalizability of using the fMRI-derived brain-aligned vectors to decode other types of neuroimaging brain data, we performed decoding and identification analyses on MEG and ECoG neural data from different participants that were exposed to the same visual stimuli. For MEG analyses, we used source-estimated signals from the ventral visual stream (see methods for source localization and detailed preprocessing procedures). For ECoG, we concatenated the high- γ power components from 4 subjects with a total of 231 electrodes implanted on their ventral visual cortex (see Methods). We trained separate linear regression models as brain decoders for each of the MEG and ECoG datasets, subjects and feature space types, using fMRI brain-aligned vectors derived from averaged RSM matrices across all 5 fMRI subjects.

Figure 4 shows the decoding and identification results of the MEG neural data. Similar to the fMRI analyses, we first determined whether the MEG data could be successfully decoded. In all analyses of the MEG data (i.e., samplewise decoding, dimensionwise decoding and identification), the real decoding accuracy was significantly greater than the corresponding

shuffled decoding accuracy ($P < 0.05$, one-sided t -test after Fisher's z transform; Fig. 4a-c; see Supplementary Tables 61-84 for exact values).

Subsequently, we evaluated the effect of using fMRI-based brain-aligned feature vectors for probing whether they can improve the samplewise and dimensionwise decoding and identification accuracies of MEG neural data. The samplewise decoding accuracy significantly differed with α (CLIP-based feature vectors, $F_{(5, 12)} = 41.587$, $P < 0.001$; GLoVe-based feature vectors, $F_{(5, 12)} = 368.447$, $P < 0.001$; one-way ANOVA, Bonferroni corrected significance level = $0.05/12$; Fig. 4a). Compared with those of the original feature vectors, the decoding accuracies of the brain-aligned vectors with $\alpha = 1$ were significantly increased (CLIP-based feature vectors, $P = 0.034$; GLoVe-based feature vectors $P < 0.0$; Tukey's HSD post hoc test; Fig. 4a). Among the CLIP-based vectors, the best decoding accuracies corresponded to the brain-aligned vectors containing the most brain-related information ($\alpha = 10^{-3}$ and $\alpha = 10^{-4}$); these decoding accuracies were significantly greater than the decoding accuracies of the original feature vectors ($P < 0.01$, Tukey's HSD post hoc test; Fig. 4a) and feature vectors with $\alpha = 1$ ($P < 0.01$, Tukey's HSD post hoc test; Fig. 4a). As α decreased within the GLoVe-based vectors, decoding accuracies corresponding to the brain-aligned vectors with $\alpha \leq 10^{-1}$ significantly exceeded that of the original feature vectors ($P < 0.01$, Tukey's HSD post hoc test; Fig. 4a), and the decoding accuracies corresponding to the brain-aligned vectors with $\alpha \leq 10^{-2}$ achieved a significantly improvement over the decoding accuracy corresponding to the vectors with $\alpha = 1$ ($P < 0.01$, Tukey's HSD post hoc test; Fig. 4a).

For the dimensionwise decoding of MEG data, only the decoding accuracies for GLoVe-based feature vectors differed across different values of α (CLIP-based feature vectors, $F_{(5, 12)} = 1.392$, $P = 0.2947$; GLoVe-based feature vectors, $F_{(5, 12)} = 4.766$, $P = 0.0125$; Fig. 4b).

Additionally, the dimensionwise decoding accuracy of the GLoVe-based brain-aligned vectors tended to increase as α decreased, and more particularly, the decoding accuracies corresponding to the feature vectors with $\alpha = 10^{-1}$, $\alpha = 10^{-2}$ and $\alpha = 10^{-4}$ significantly increased compared with the dimensionwise decoding accuracy of the original GLoVe feature vectors ($P < 0.05$, Tukey's HSD post hoc test; Fig. 4b).

Furthermore, the identification results for the MEG data showed significant differences with different values of α (CLIP-based feature vectors, $F_{(5, 12)} = 23.130$, $P < 0.001$; GLoVe-based feature vectors, $F_{(5, 12)} = 125.602$, $P < 0.001$; Fig. 4a). For the CLIP-based vectors, the identification accuracies corresponding to the brain-aligned vectors with $\alpha = 1$ and $\alpha = 10^{-1}$ decreased compared with the identification accuracies of the original feature vectors ($P < 0.01$, Tukey's HSD post hoc test; Fig. 4c); however, the identification accuracies corresponding to the vectors containing more brain-related information ($\alpha = 10^{-2}$, $\alpha = 10^{-3}$ and $\alpha = 10^{-4}$) significantly increased compared with the identification accuracies of the brain-aligned feature vectors with $\alpha = 1$ ($P < 0.01$, Tukey's HSD post hoc test; Fig. 4c). For the GLoVe-based vectors, the identification accuracies corresponding to the brain-aligned vectors with $\alpha \leq 1$ were significantly increased compared with the identification accuracy of the original feature vectors ($P < 0.01$, Tukey's HSD post hoc test; Fig. 4a), and the identification accuracies corresponding to the brain-aligned vectors with $\alpha = 10^{-2}$ and $\alpha = 10^{-3}$ were significantly greater than the identification accuracy corresponding to the vectors with $\alpha = 1$ ($P < 0.05$, Tukey's HSD post hoc test; Fig. 4c); however, the identification accuracies corresponding to the brain-aligned vectors with $\alpha = 10^{-1}$ and $\alpha = 10^{-4}$ were significantly lower than the identification accuracy corresponding to the vectors with $\alpha = 1$ ($P < 0.05$, Tukey's HSD post hoc test; Fig. 4c; see supplementary Fig. 2 and supplementary tables 85-90).

Remarkably, with the ECoG data, we observed that the samplewise and dimensionwise decoding accuracies of the brain-aligned vectors with $\alpha = 10^{-4}$ were the highest and were improved over both the original feature vectors and the brain-aligned vectors with $\alpha = 1$ (Fig. 5a and b). Additionally, the identification accuracy of brain-aligned vectors with $\alpha = 10^{-4}$ was increased compared with the identification accuracy of the original vectors for both CLIP-based and GLoVe-based feature vectors (Fig. 5c).

Discussion

Here, we demonstrated the ability of our proposed brain-aligning method to enhance zero-shot brain decoding across diverse neuroimaging datasets and distinct individuals. Notably, the fMRI brain decoders trained on the CLIP-based and GLoVe-based brain-aligned feature vectors outperformed those trained on the original pretrained vectors, particularly when utilizing vectors that underwent the highest level of brain-aligning (brain-aligned vectors with $\alpha = 10^{-4}$) (Fig. 3a and b). Critically, this improvement was observed even when considering other types of neuroimaging neural data (MEG and ECoG), subjects, and stimulus categories that were not included in training the brain-aligning model (Figs. 4a and b, and 5a and b), highlighting the robustness and generalizability of our approach. Furthermore, the brain-aligning process did not reduce identification accuracy in either case, reinforcing the potential of this technique for real-world applications requiring both precise decoding and identification (Figs. 3e and f, and 4c and 5c).

Previous studies have attempted to develop a brain-based semantic representation space. For example, Binder *et al.*⁴⁵ proposed a model where word meanings are represented as combinations of basic sensory, motor, affective, and cognitive experiences. They proposed a

basic set of approximately 65 experiential attributes on the basis of neurobiological considerations, comprising sensory, motor, spatial, temporal, affective, social, and cognitive experiences and collected normative data on these experiential attributes to create a semantic space based on real brain activity. In another study, Chersoni *et al.*⁴⁶ advanced this concept by demonstrating the decoding of word embeddings using brain-based semantic features derived from fMRI data. However, while Binder *et al.*⁴⁵ established a foundation for linking brain activity to semantic representations, their approach relied on manually-defined attributes rather than directly utilizing the raw neural data. In contrast, our approach harnesses the inherent structure of neural representations by directly using the second-order statistical characteristics of brain activity patterns, avoiding the need for manual attribute definitions. This data-driven approach may offer a more direct and potentially comprehensive representation of neural semantic space.

In addition to creating brain-based semantic spaces, as exemplified by Binder *et al.*⁴⁵, several studies have fine-tuned neural representations with human, monkey or rat brain-based information to enhance performance on downstream tasks. For example, Federer *et al.*³² reported that training neural networks to mimic the statistical properties of brain activity can improve object recognition. Later, Li *et al.*⁴⁷ integrated deep neural network features with brain network information to enhance the prediction of brain activity during naturalistic perception. Additionally, Muttenthaler *et al.*³³ explored aligning neural network representations with human similarity judgments to improve few-shot learning and anomaly detection. Finally, Schneider *et al.*³⁴ demonstrated the power of combining behavioral and neural data through latent embeddings for predicting behavior. However, despite these advancements, these previous studies did not explicitly explore fine-tuning pretrained feature vectors to directly match the second-order

statistical representations of human brain activity, nor did they systematically investigate the resulting zero-shot decoding performance on new subjects and neuroimaging modalities. Our brain-aligning method addresses this gap by aligning feature vector relationships with those observed in neural responses, demonstrating robust cross-modality and cross-subject decoding capabilities.

Our findings are also aligned with the broader literature addressing hyperalignment⁴⁸ and the need to discover shared neural representational spaces across individuals. While our primary goal was not to derive a common high-dimensional space *per se*, our results nevertheless suggest a degree of alignment across individuals. By creating brain-aligned vectors on the basis of averaged representational similarity matrices (RSMs) across subjects, we effectively leveraged the neural representations that are common across individuals. The subsequent successful decoding of neural activity patterns from a different set of subjects aligns with previous findings such as those of Guntupalli *et al.*⁴⁹ who demonstrated the feasibility of finding such shared spaces even at a fine-grained, searchlight level. Furthermore, our results expand upon the notion of shared representations across neuroimaging modalities, consistent with findings from studies such as Haxby *et al.*⁴⁸ that suggest the existence of common representational structures in fMRI data. Notably, in our study, the successful decoding of MEG and even ECoG signals via our fMRI-derived brain-aligned vectors provides evidence for a shared representational space with consistent second-order statistical characteristics across these distinct modalities.

In conclusion, our study demonstrates the notable potential of brain-aligning semantic vectors in increasing the accuracy and generalizability of neural decoding algorithms. By integrating brain-related information into pretrained feature vectors, we achieved robust zero-shot decoding performance across different individuals and neuroimaging modalities, even with

a relatively small fMRI dataset (consisting of approximately 150 categories). This suggests that our approach efficiently captures essential neural representations even with limited training data. While these results are promising, future exploration of several issues is needed. For example, investigating the impact of different autoencoder architectures, training strategies, loss metrics, and leveraging larger datasets could further optimize the effectiveness of brain-aligning vectors. Additionally, developing methods to mitigate potential biases in the brain-aligning process and enhance the interpretability of the resulting vectors would facilitate real-world applications. Beyond these immediate refinements, future work could explore the application of brain-aligning to a broader range of cognitive domains and tasks, ultimately paving the way for more powerful and versatile brain-machine interface technologies.

Methods

Creating semantic vectors

Semantic vectors are multidimensional representations of data that encode the underlying semantics, relationships, and context within that data. These vectors have been widely used for brain decoding as meaningful representations of stimuli, thus training decoders to map neural activity patterns to corresponding semantic vector representations. Here, we used two different types of semantic spaces that have been previously used in brain decoding studies. Specifically, we use pretrained feature vectors from the last layer of the CLIP image encoder and pretrained feature vectors from the GloVe model. We created semantic vectors for all categories in the ImageNet dataset fall 2011 release³³.

GloVe

GloVe is a method that can generate 300-dimensional semantic vector representations of a given word from a normalized version of the statistical results of word cooccurrences obtained from a corpus with more than 42 billion tokens. Words with similar meanings are associated with vectors that are close in the vector space, enabling GLoVe to capture the semantic meaning of words and their contextual associations. Here, we used the pretrained word vectors of the 42B token file (<https://nlp.stanford.edu/data/glove.42B.300d.zip>). For each image category in the ImageNet dataset, we considered their annotations obtained by crowdsourcing³³ and calculated the average GLoVe representations of all available annotations in the GloVe dictionary as a representation of that category. If any of the annotations of a particular category did not exist in the GLoVe dictionary, that category was excluded from all subsequent analyses.

CLIP

CLIP is a model that connects vision and language by generating semantic vectors for both images and text. The unique advantage of using CLIP lies in its ability to map images and textual descriptions into a shared vector space, where the similarity or dissimilarity between vectors accurately reflects the semantic relationships between the two modalities. To create a CLIP semantic vector for each category in ImageNet, we extracted an image from each category and then extracted the features from the ViT-B/32 transformer image encoder of the CLIP model for that image.

fMRI dataset

Dataset description

We made use of one publicly available dataset, commonly referred to as the “Generic Object Decoding” dataset¹⁸. Five healthy subjects (one female and four males, aged between 23 and 38 years) with normal or corrected-to-normal vision participated in the experiments. The experiments consisted of presenting natural object images to the subjects and recording their brain activity while they viewed the visual stimuli (perception experiment) or imagined them (imagery experiment). Images were selected from the ImageNet dataset. The training dataset consisted of neural recordings of 1200 images (150 categories, 8 images per category), all of which were viewed by the participants. The test dataset consisted of neural recordings of 50 perceived and 50 imagined images (50 images were selected from 50 categories, i.e., 1 image per category, and were not used in the training dataset; the training and test images were presented 35 and 10 times, respectively), and the study protocol was approved by the Ethics Committee of the ATR. The LOC brain region was identified via the functional localizer experiment and SPM5 software.

MEG dataset

MEG experiment

MEG experiments were conducted within our laboratory. Three subjects (3 males, aged between 25 and 34) viewed images from the GOD dataset, and their brain activity was recorded via MEG. Participants viewed the images during the experiment. Each of the images in the training or test dataset was repeated 6 times, and the participants were asked to fixate on a central dot on the images. The study adhered to the Declaration of Helsinki and was performed in accordance with

protocols approved by the ethics committee of our University Clinical Trial Center (No. 18472-5). All the participants provided informed consent.

MEG preprocessing

First, the raw MEG data were imported into Brainstorm⁴¹, a specialized software tool for neuroimaging analysis. To eliminate unwanted frequency components, essential filters, including a high-pass filter at 0.5 Hz and a notch filter at 60 Hz and its harmonics, were subsequently employed. To address potential cardiac and blink artifacts, independent component analysis (ICA) was employed. The robustness of the analysis was further enhanced by the use of room data to compute noise covariance and generate a subject-specific head model from individual MRI data. This enabled the accurate estimation of neural sources in the brain. Following source estimation, individual source activities were projected onto the default brain model (FSAverage) for consistency. To precisely mark the onset of each stimulus, analog triggers were utilized. After these preprocessing steps, a high-quality dataset was obtained in the form of a matrix with dimensions of 200 samples (equivalent to milliseconds) by 7200 trials by 15002 vertices. The sensorimotor cortical potential (SCP) was subsequently calculated by averaging signals within specific time windows, resulting in a 7200×15002 matrix that served as the foundation for subsequent analyses.

MEG ROI selection

Region of interest (ROI) selection consisted of two steps. First, the neural sources of the recorded MEG signals were estimated through a process called source localization⁴². These source-localized data were then anatomically registered to the brain parcellation of the Human

Connectome Project (HCP)⁴³. Here, we selected source-localized data from the ventral visual cortex (VSVC). All the abovementioned processes were performed using Brainstorm.

ECoG dataset

Experimental settings

The experiments were conducted in a cohort of epilepsy patients who had undergone neurosurgical procedures for the implantation of intracranial electrodes to localize the epileptogenic zones responsible for seizure onset. During the experiments, the subjects either sat on beds in their hospital rooms or were seated on chairs in front of a computer screen to watch the visual stimuli. The intracranial brain signals from each subject were recorded with an EEG-1200 system (Nihon Koden, Tokyo, Japan) with a sampling rate of 10 kHz. Digital triggers encoding the presentation timing of the visual stimuli were generated by DATAPixx3 (VPixx Technologies, Quebec, Canada) and recorded synchronously with the ECoG signals. The experiment adhered to the Declaration of Helsinki and was performed in accordance with protocols approved by the ethics committee of our University Clinical Trial Center (No. 14353). All the participants provided informed consent.

Experimental procedures

Seventeen subjects participated in the image presentation task. These tasks were completed in 2 to 4 recording sessions over 1 to 3 days. To compensate for session-to-session changes in electrode impedance, baseline ECoG recordings were performed separately at the beginning of each recording session. Four subjects from this cohort were selected for further analysis on the

basis of two criteria: 1) the presence of electrodes implanted on their ventral visual cortex and 2) demonstration of initial decoding performance exceeding chance levels. The numbers of electrodes in these four subjects were 74, 56, 30, and 71, respectively.

Baseline recording task

To compensate for the session-to-session differences in electrode impedance, a baseline recording was performed at the beginning of each recording session. The task consisted of one run, in which the subjects were presented with images from a baseline image dataset in random order with no presentation of a blank screen between the images. The subjects were instructed to view the presented images while keeping their eyes on a red fixation point at the center of the screen. The duration of the presentation of each image was 1100 ms.

Image presentation task

In the image presentation task, the GOD image dataset was presented to the subjects as a visual stimulus. The GOD training images and evaluation images were presented in two and one runs, respectively, although the structure of the runs was the same. Each subject participated in one or multiple training and evaluation runs. In each run, 10 images of the preceding stimuli image dataset were first presented in random order, followed by images from the GOD image dataset, which were also presented in random order. There was no presentation of a blank screen between the presentations of the images. The duration of the presentation of each image was 500 ms. During this task, the subjects were instructed to view the images with their eyes on the red fixation point in the center of the screen. The division of the GOD training images for the two

runs was randomized for each pair of runs, and the corresponding runs in a pair were always performed in the same recording session.

ECoG preprocessing

For each subject, we performed a visual inspection of the raw data and removed data from noisy channels. Common average referencing was then applied to mitigate common noise sources and accentuate local neural activity. ECoG epochs, which were time-locked to stimulus onset and extended 0.5 seconds poststimulus, were extracted to focus on stimulus-related processing. Power spectral density (PSD) analysis was performed on each epoch, and the high gamma power component (80-150 Hz) was extracted as the feature of interest because of its established association with cognitive processes. These high gamma data subsequently served as inputs for statistical analyses investigating neural activity patterns in relation to experimental conditions. Finally, we concatenated the data corresponding to electrodes that were placed in the ventral visual stream of patients as the final ECoG data.

Autoencoder framework

The autoencoder consists of two fully connected layers with ReLU activation functions. The number of dimensions in the autoencoder's latent space was set to half the number of dimensions of the original vectors. For each subject, brain region and semantic space type, a separate autoencoder was trained. When training the autoencoder for a particular subject, we used the averaged brain RSMs of all other subjects. After we finished the training process, we input all the original semantic vectors to the trained model and used the intermediate features of the resulting trained autoencoder as the brain-aligned features.

The RSM matrices were created from the brain activity pattern or the autoencoder’s latent space by calculating the pairwise cosine similarity of each of the two data points. During the training process, we used the difference between the upper triangle of each of the RSM matrices to constrain the autoencoder to make representations more brain-like.

Neural decoding of visual stimuli

We performed brain decoding by constructing linear regression models to predict semantic vectors from brain activity patterns. To predict each unit of semantic vectors, a separate set of linear regression models was trained. Prior to regression analysis, we performed voxel selection via a method similar to that used by Horikawa and Kamitani¹⁵, and the brain activity patterns were Z-normalized.

More formally, given brain activity patterns as $x = \{x_1, x_2, \dots, x_n\}^T$ representing the activity of n neural activity data points (i.e., voxels in the fMRI data, source estimated neural activity patterns from MEG sensors, neural amplitude recorded from each channel in each second in the ECoG) from the region of interest, the regression function can be represented as:

$$y(x) = \sum_{i=1}^n w_i x_i + w_0$$

where x_i is a scalar value specifying the amplitude of the brain data point i , w_i is the weight of voxel i and w_0 is the bias.

For each subject, semantic space type and brain region, we trained a separate set of linear regression functions as decoders. When decoding fMRI data of a particular subject to the brain-aligned semantic spaces, we used the brain-aligned space in which that subject was not used to

create. When decoding the MEG data of a particular subject, we used the averaged brain-aligned semantic spaces of all fMRI subjects.

Identification analysis

For the identification analysis, the final predicted vector was identified among a large set of candidate vectors. First, we prepared one random image from each class of the ImageNet dataset. Then, for each semantic space (i.e., the GloVe- and CLIP-based pretrained feature vectors or the GLoVe- and CLIP-based brain-aligned vectors for different values of α), we calculated the corresponding semantic vectors of all images that we had been randomly selected from ImageNet. If we could not obtain the GLoVe embeddings of a category, that category was excluded from all analyses. When obtaining the brain-aligned vectors of all ImageNet categories, we input the original GLoVe/CLIP pretrained feature vectors to the corresponding trained autoencoder and obtained the corresponding brain-aligned vectors. Then, for each category in the GOD dataset, we calculated the Pearson correlation coefficient of the true and predicted vectors and the predicted vector and all other candidate vectors and assigned the identification accuracy as the percentage of candidate categories, in which their correlation with the test predicted vector is lower than the correlation of the true and predicted vectors. The chance-level identification accuracy was determined by randomly shuffling the true feature vectors and calculating the identification accuracy for the shuffled vectors, following the same procedure as for the unshuffled data.

Statistical test

In the decoding analyses, we evaluated the performance of the brain decoders using the Pearson correlation coefficients of the predicted and true feature vectors, as well as between the predicted and shuffled true feature vectors. Then, we applied Fisher's z-transform to the correlations of each case to stabilize variance, followed by one-sided t -tests for each feature space type and neuroimaging modality. Similarly, in the identification analysis, we performed a one-sided t -test between the identification results of shuffled data and unshuffled data.

To compare the decoding and identification accuracy means among the original feature vectors and brain-aligned feature vectors, we applied a one-way analysis of variance (ANOVA) followed by Tukey's honestly significant difference (HSD) post hoc test. Prior to each t -test and ANOVA, we assessed the normality of the data via the Shapiro–Wilk test.

To calculate the significant differences in F value distributions among different types of CLIP-based feature vectors (original vs. brain-aligned), we applied the two-sided Wilcoxon rank-sum test between each pairwise combination of original and/or brain-aligned feature vectors.

References

1. Stavisky, S. D. & Wairagkar, M. Listening in to perceived speech with contrastive learning. *Nat. Mach. Intell.* **5**, 1179-1180 (2023).
2. Lebedev, M. A. & Nicolelis, M. A. Brain-machine interfaces: past, present and future. *Trends Neurosci.* **29**, 536-546 (2006).
3. Willett, F. R. et al. A high-performance speech neuroprosthesis. *Nature* **620**, 1031-1036 (2023).
4. Willsey, M. S. et al. Real-time brain-machine interface in non-human primates achieves high-velocity prosthetic finger movements using a shallow feedforward neural network decoder. *Nat. Commun.* **13**, 6899 (2022).
5. Haynes, J. D. & Rees, G. Decoding mental states from brain activity in humans. *Nat. Rev. Neurosci.* **7**, 523-534 (2006).
6. Naselaris, T., Kay, K. N., Nishimoto, S. & Gallant, J. L. Encoding and decoding in fMRI. *Neuroimage* **56**, 400-410 (2011).
7. Haxby, J. V. et al. Distributed and overlapping representations of faces and objects in ventral temporal cortex. *Science* **293**, 2425-2430 (2001).
8. Yamins, D. L. et al. Performance-optimized hierarchical models predict neural responses in higher visual cortex. *Proc. Natl. Acad. Sci. U. S. A.* **111**, 8619-8624 (2014).
9. Kellis, S. et al. Decoding spoken words using local field potentials recorded from the cortical surface. *J. Neural Eng.* **7**, 056007 (2010).
10. Brouwer, G. J. & Heeger, D. J. Decoding and reconstructing color from responses in human visual cortex. *J. Neurosci.* **29**, 13992-14003 (2009).

11. Sitaram, R. et al. Closed-loop brain training: the science of neurofeedback. *Nat. Rev. Neurosci.* **18**, 86-100 (2017).
12. Fukuma, R. et al. Voluntary control of semantic neural representations by imagery with conflicting visual stimulation. *Commun. Biol.* **5**, 214 (2022).
13. Chaudhary, U. et al. Spelling interface using intracortical signals in a completely locked-in patient enabled via auditory neurofeedback training. *Nat. Commun.* **13**, 1236 (2022).
14. Cortese, A., Amano, K., Koizumi, A., Kawato, M. & Lau, H. Multivoxel neurofeedback selectively modulates confidence without changing perceptual performance. *Nat. Commun.* **7**, 13669 (2016).
15. Horikawa, T. & Kamitani, Y. Generic decoding of seen and imagined objects using hierarchical visual features. *Nat. Commun.* **8**, 15037 (2017).
16. Haynes, J. D. & Rees, G. Predicting the orientation of invisible stimuli from activity in human primary visual cortex. *Nat. Neurosci.* **8**, 686-691 (2005).
17. Kamitani, Y. & Tong, F. Decoding the visual and subjective contents of the human brain. *Nat. Neurosci.* **8**, 679-685 (2005).
18. Thirion, B. et al. Inverse retinotopy: inferring the visual content of images from brain activation patterns. *Neuroimage* **33**, 1104-1116 (2006).
19. Cox, D. D. & Savoy, R. L. Functional magnetic resonance imaging (fMRI) "brain reading": detecting and classifying distributed patterns of fMRI activity in human visual cortex. *Neuroimage* **19**, 261-270 (2003).
20. Nakai, T., Koide-Majima, N. & Nishimoto, S. Correspondence of categorical and feature-based representations of music in the human brain. *Brain Behav.* **11**, e01936 (2021).

21. Koide-Majima, N., Nishimoto, S. & Majima, K. Mental image reconstruction from human brain activity. *BiorXiv*. <https://doi.org/10.1101/2023.01.22.525062> (2023).
22. Miyawaki, Y. et al. Visual image reconstruction from human brain activity using a combination of multiscale local image decoders. *Neuron* **60**, 915-929 (2008).
23. Shen, G., Dwivedi, K., Majima, K., Horikawa, T. & Kamitani, Y. End-to-end deep image reconstruction from human brain activity. *Front. Comput. Neurosci.* **13**, 21 (2019).
24. Shen, G., Horikawa, T., Majima, K. & Kamitani, Y. Deep image reconstruction from human brain activity. *PLoS Comput. Biol.* **15**, e1006633 (2019).
25. Krizhevsky, A., Sutskever, I. & Hinton, G. E. ImageNet classification with deep convolutional neural networks in *Advances in Neural Information Processing Systems* (eds Pereira, F., Burges, C. J., Bottou, L. & Weinberger, K. Q.) 1097-1105 (Curran Associates, Inc., Red Hook, NY, 2012).
26. Liu, Y., Ma, Y., Zhou, W., Zhu, G. & Zheng, N. BrainCLIP: bridging brain and visual-linguistic representation via CLIP for generic natural visual stimulus decoding. <https://doi.org/10.48550/arXiv.2302.12971> (2023).
27. Radford, A. et al. Learning transferable visual models from natural language supervision in *International Conference on Machine Learning* 8748-8763 (PMLR, Virtual Event, 2021).
28. Pereira, F. et al. Toward a universal decoder of linguistic meaning from brain activation. *Nat. Commun.* **9**, 963 (2018).
29. Mikolov, T., Chen, K., Corrado, G. & Dean, J. Efficient estimation of word representations in vector space. <https://doi.org/10.48550/arXiv.1301.3781> (2013).

30. Pennington, J., Socher, R. & Manning, C. D. GloVe: Global vectors for word representation in *Proceedings of the 2014 Conference on Empirical Methods in Natural Language Processing (EMNLP)* 1532-1543 (Association for Computational Linguistics, Doha, Qatar, 2014).
31. Shirakawa, K. et al. Spurious reconstruction from brain activity. <https://doi.org/10.48550/arXiv.2405.10078> (2024).
32. Federer, C., Xu, H., Fyshe, A. & Zylberberg, J. Improved object recognition using neural networks trained to mimic the brain's statistical properties. *Neural Netw.* **131**, 103-114 (2020).
33. Muttenthaler, L. et al. Improving neural network representations using human similarity judgments. <https://doi.org/10.48550/arXiv.2306.04507> (2023).
34. Schneider, S., Lee, J. H. & Mathis, M. W. Learnable latent embeddings for joint behavioural and neural analysis. *Nature* **617**, 360-368 (2023).
35. Kay, K. N., Naselaris, T., Prenger, R. J. & Gallant, J. L. Identifying natural images from human brain activity. *Nature* **452**, 352-355 (2008).
36. Ogawa, S., Lee, T. M., Kay, A. R. & Tank, D. W. Brain magnetic resonance imaging with contrast dependent on blood oxygenation. *Proc. Natl. Acad. Sci. U. S. A.* **87**, 9868-9872 (1990).
37. Penfield, W. & Jasper, H. *Epilepsy and the Functional Anatomy of the Human Brain* (Little, Brown & Co., Oxford, UK, 1954).
38. Cohen, D. Magnetoencephalography: evidence of magnetic fields produced by alpha-rhythm currents. *Science* **161**, 784-786 (1968).

39. Deng, J. et al. ImageNet: a large-scale hierarchical image database in *2009 IEEE Conference on Computer Vision and Pattern Recognition* 248-255 (IEEE, Miami, FL, 2009).
40. Kourtzi, Z. & Kanwisher, N. Cortical regions involved in perceiving object shape. *J. Neurosci.* **20**, 3310-3318 (2000).
41. Norman, K. A., Polyn, S. M., Detre, G. J. & Haxby, J. V. Beyond mind-reading: multi-voxel pattern analysis of fMRI data. *Trends Cogn. Sci.* **10**, 424-430 (2006).
42. Cichy, R. M., Pantazis, D. & Oliva, A. Resolving human object recognition in space and time. *Nat. Neurosci.* **17**, 455-462 (2014).
43. Horikawa, T., Tamaki, M., Miyawaki, Y. & Kamitani, Y. Neural decoding of visual imagery during sleep. *Science* **340**, 639-642 (2013).
44. Mitchell, T. M. et al. Predicting human brain activity associated with the meanings of nouns. *Science* **320**, 1191-1195 (2008).
45. Binder, J. R. et al. Toward a brain-based componential semantic representation. *Cogn. Neuropsychol.* **33**, 130-174 (2016).
46. Chersoni, E., Santus, E., Huang, C. R. & Lenci, A. Decoding word embeddings with brain-based semantic features. *Comput. Linguist.* **47**, 663-698 (2021).
47. Li, Y., Yang, H. & Gu, S. Enhancing neural encoding models for naturalistic perception with a multi-level integration of deep neural networks and cortical networks. *Sci. Bull. (Beijing)* **69**, 1738-1747 (2024).
48. Haxby, J. V. et al. A common, high-dimensional model of the representational space in human ventral temporal cortex. *Neuron* **72**, 404-416 (2011).

49. Guntupalli, J. S. et al. A model of representational spaces in human cortex. *Cereb. Cortex* **26**, 2919-2934 (2016).

Acknowledgements

We thank all subjects for their participation. This research was supported by the Japan Science and Technology Agency (JST) Moonshot R&D (JPMJMS2012), JST Core Research for Evolutional Science and Technology (CREST) (JPMJCR18A5), JST AIP Acceleration Research (JPMJCR24U2), and Japan Society for the Promotion of Science (JSPS) Grants-in-Aid for Scientific Research (KAKENHI) (JP26560467 and JP20H05705).

Author contributions

S.V., R. F. and T.Y. conceptualized the project. S.V. was responsible for the theory. S.V., R.F. and T.Y. were responsible for the methodology. S.V. undertook the analysis and investigation. R. F. and H. Y. were responsible for the MEG and ECoG experiments. S.V. was responsible for data preprocessing and curation. S.V. wrote the original draft and created the figures. S.V. and T.Y. edited the final version of the article. S.O., N.T., H.M.K., H.S., Y.I., H.S., M.N. and K.T. performed the neurosurgery of ECoG experiments

Competing interests

The authors declare that they have no competing interests.

Data Availability

The datasets supporting the findings of this study include fMRI, MEG, and ECoG data. The fMRI dataset used in this study is already available at <https://openneuro.org/datasets/ds001246/versions/1.0.0>. MEG data will be made publicly available after publication on Figshare (https://figshare.com/**/). The ECoG features used in

this study will be available on Figshare (URL to be provided), and the raw signals of ECoG will be available under a formal data-sharing agreement. For inquiries about data before it is uploaded, please contact the corresponding author.

Code Availability

The code used for data analysis in this study will become publicly available on our GitHub repository (<https://github.com/yanagisawa-lab>) at the time of publication. For inquiries about code before it is uploaded, please contact the corresponding author.

Figures and Figure legends

Fig. 1

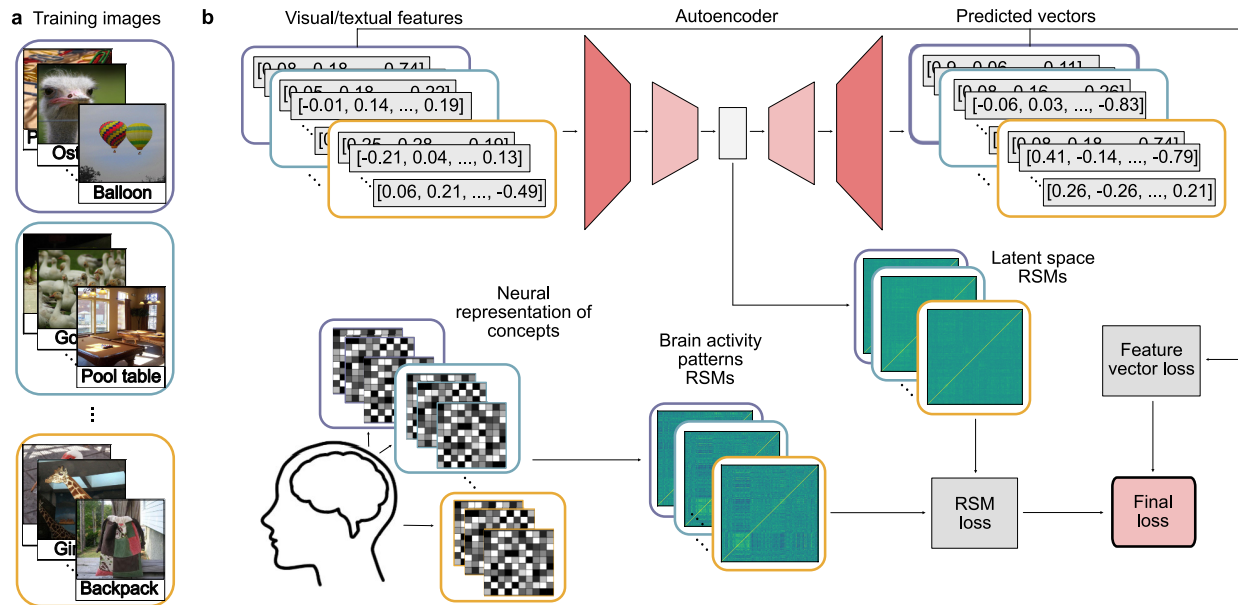


Fig. 1. Examples of the visual stimuli and workflow of the brain-aligning framework. (a) Samples images from the GOD dataset. The rectangles represent the sample image batches used for training. **(b)** The brain-aligning framework. First, pretrained visual or textual features are extracted. Then, an autoencoder is trained to reconstruct these features while aligning the representational similarity matrix (RSM) of its latent space with the RSM of corresponding brain activity patterns.

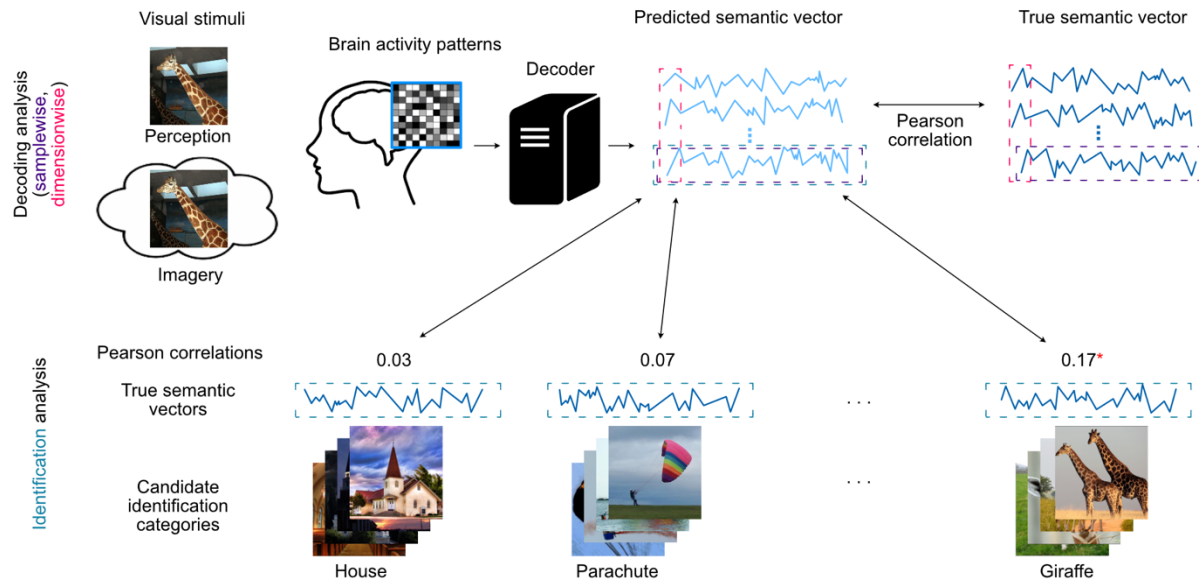


Fig. 2. Decoding and identification procedure. Brain decoders are trained to map brain activity patterns associated with a visual stimulus to their corresponding feature vectors. In the identification analysis, a large set of candidate stimuli is considered. The Pearson correlation coefficient is calculated between the predicted semantic vector and the semantic vectors of each candidate stimulus, facilitating identification of the most likely perceived or imagined stimulus.

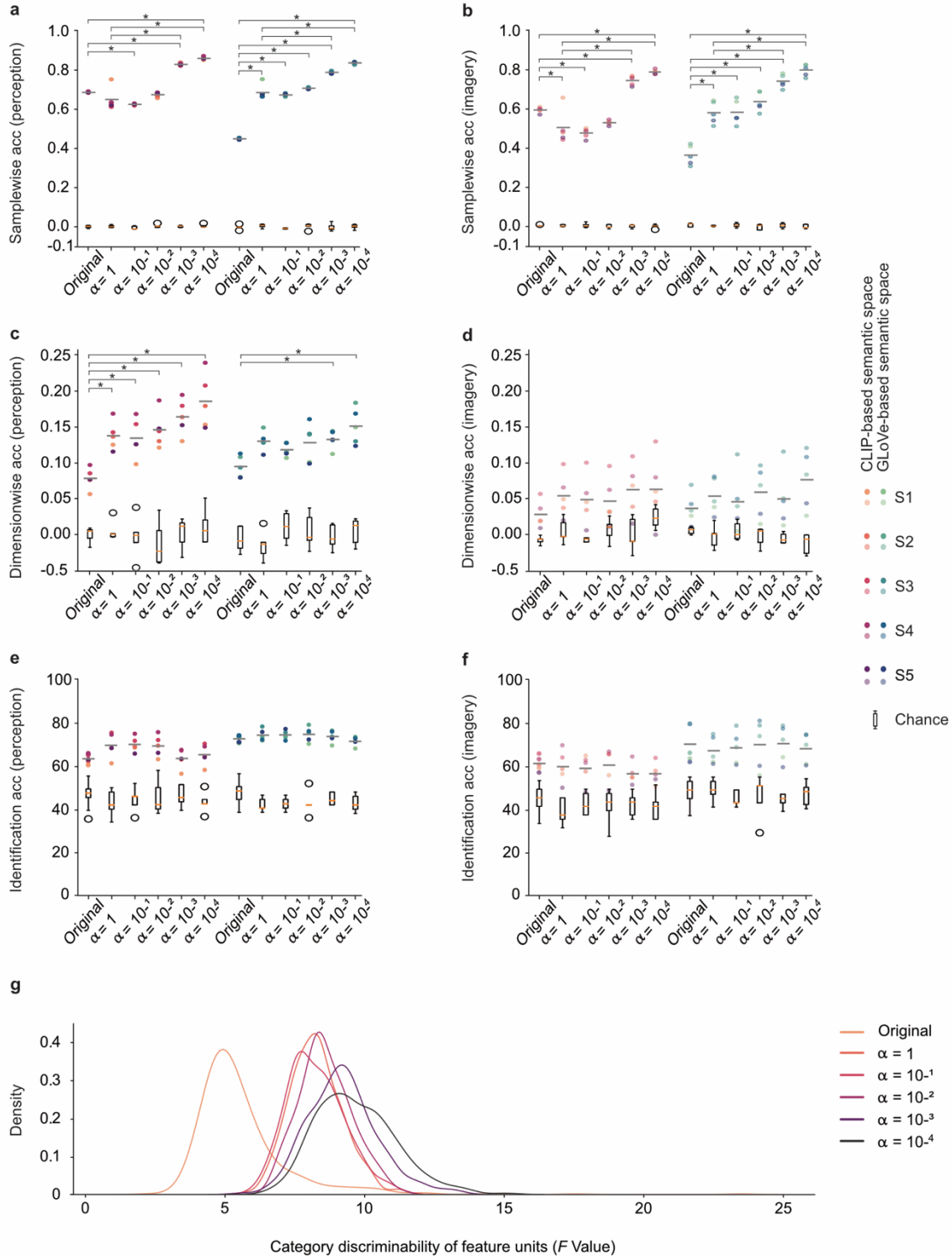


Fig. 3. fMRI decoding and identification results. fMRI decoding and identification results of perceived and imagined image data into the original and brain-aligned feature vectors of CLIP

and GloVe, evaluated by **(a and b)** samplewise decoding accuracy, **(c and d)** dimensionwise decoding accuracy, and **(e and f)** identification accuracy. For clarity, only the significant differences between the brain-aligned vectors with the original pretrained feature vectors and with the brain-aligned vectors with $\alpha = 1$ are indicated with an *. For all pairwise significant results, see the Supplementary Fig. 1. **(g)** Distribution of category discriminability of original and brain-aligned CLIP-based feature vectors.

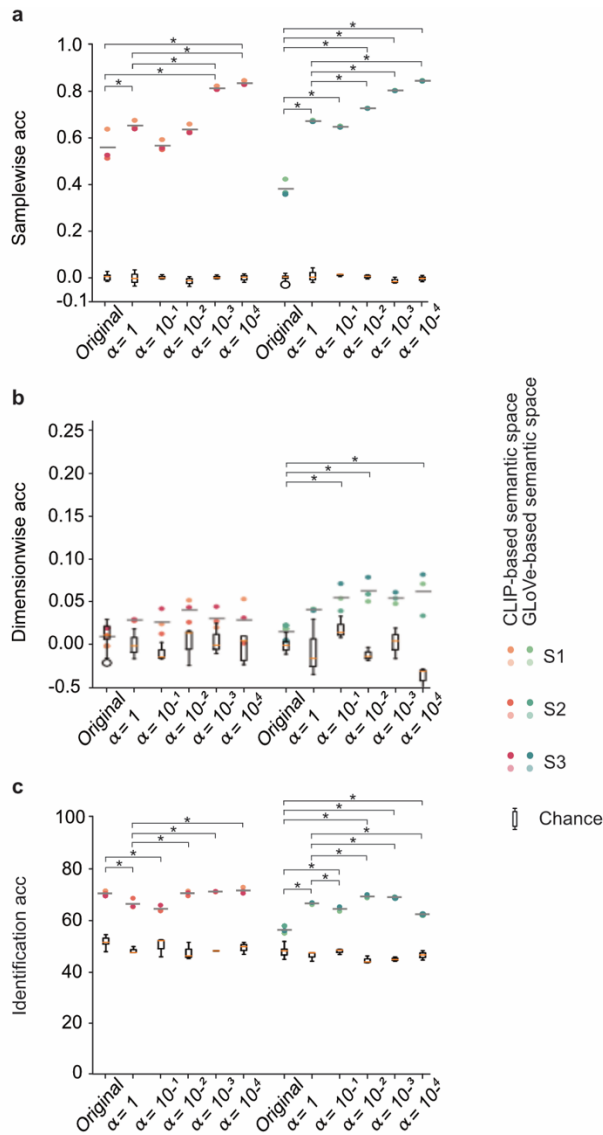


Fig. 4. Decoding and identifying perceptual content from MEG neural data. Perceptual content is decoded and identified from MEG neural recordings via original and brain-aligned CLIP- and GloVe-based feature vectors. Decoding accuracy is assessed via (a) samplewise and (b) dimensionwise measurements. (c) shows the MEG identification results. For clarity, only the significant differences between the brain-aligned vectors and the original pretrained feature vectors or the brain-aligned vectors with $\alpha = 1$ are depicted. For all the results, see Supplementary Fig. 2.

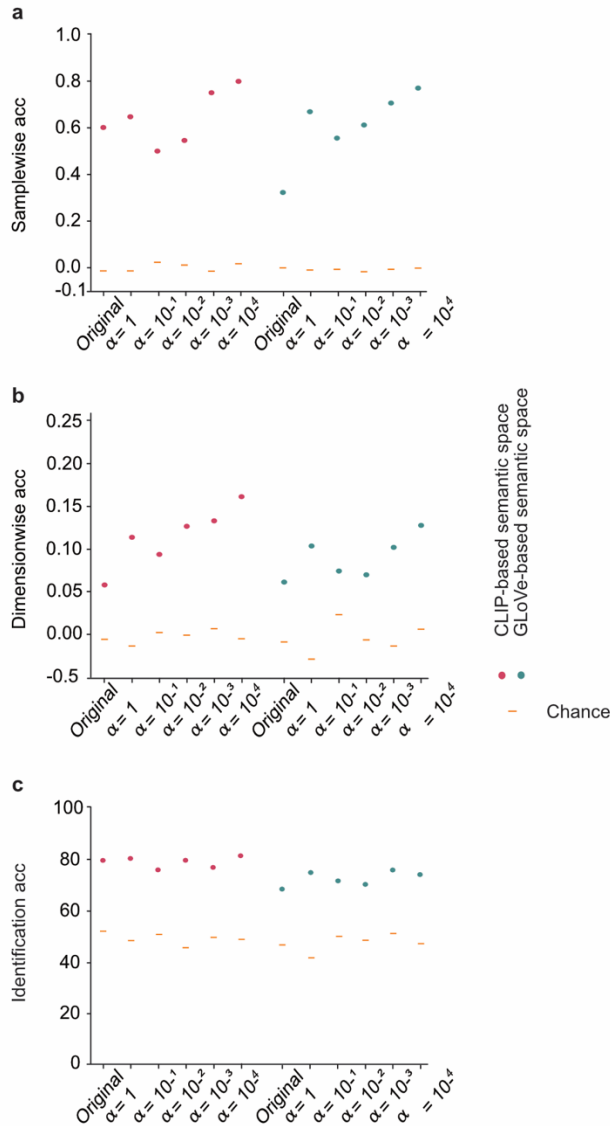


Fig. 5. Decoding and identifying perceptual content from ECoG neural recordings. Visual stimuli are decoded and identified from ECoG recordings using original and brain-aligned CLIP- and GloVe-based feature vectors. Decoding accuracy is assessed via (a) samplewise and (b) dimensionwise measurements. (c) depicts the identification results. The dots represent the decoding/identification accuracy of the concatenated ECoG subjects.